AIMS Mathematics, 9(1): 702–722.
DOI: 10.3934/math.2024036
Received: 16 August 2023
Revised: 23 October 2023
Accepted: 13 November 2023
Published: 04 December 2023

http://www.aimspress.com/journal/Math

Research article

Numerical solution of unsteady elastic equations with C-Bézier basis functions

Lanyin Sun* **and Kunkun Pang**

School of Mathematics and Statistics, Xinyang Normal University, Xinyang 464000, China

* **Correspondence:** Email: lysun@xynu.edu.cn.

Abstract: In this paper, the finite element method is applied to solve the unsteady elastic equations, C-Bézier basis functions are used to construct the shape function spaces, the semi-discrete scheme of the unsteady elastic equations is obtained by Galerkin finite element method and then the fully discretized Galerkin method is obtained by further discretizing the time variable with θ-scheme finite difference. Furthermore, for several numerical examples, the accuracy of approximate solutions are improved by 1–3 order-of magnitudes compared with the Lagrange basis function in L^∞ norm, L^2 norm and H^1 semi-norm, and the numerical examples show that the method proposed possesses a faster convergence rate. It is fully demonstrated that the C-Bézier basis functions have a better approximation effect in simulating unsteady elastic equations.

Keywords: unsteady elastic equation; finite element method; C-Bézier basis functions
Mathematics Subject Classification: 65D18, 65M60

1. Introduction

Unsteady elastic equations are widely used to describe many engineering and physical problems. Since it is usually difficult to get analytic solutions, numerical analysis plays a vital role in solving unsteady elastic equations. There are several numerical methods, such as finite element method (FEM) [1, 2], finite difference method (FDM) [3, 4], finite volume method (FVM) [5, 6] and spectral method (SM) [7], etc. Among them, the FEM has attracted much attention because it has strong problem-solving ability, a standardized form of discrete equations and easy preparation of general computer programs.

FEM is an important tool to solve partial differential equations (PDEs) in the field of scientific and engineering computing. In 1943, Courant [8] first proposed FEM and used piecewise linear functions to construct the Galerkin projection space. In 1960, Clough [9] formally presented the name of "finite element method" when dealing with plane elastic problems. In the 1960s, Feng [10] combined with

the stress problems of dam construction, carried out the research on the numerical solutions of elliptic boundary value problems and put forward the difference scheme based on variational principle. Based on the traditional FEM, scholars have also put forward many new numerical methods, such as mixed finite element method [11, 12], weak Galerkin finite element method [13, 14], multi scale method [15] and so on. Liu et al. [16] proposed the smoothed finite element method based on the finite element method and the meshless method. Cheng et al. [17] used the local discontinuous finite element method to deal with singular perturbation unsteady problems. Lin et al. [18] presented a streamline upwind Petrov-Galerkin (SUPG) stabilized space time finite element method for convection-diffusion-reaction equations. Varma et al. [19] analyzed the posteriori error of the adaptive finite element method for the unsteady convection-diffusion reaction equations.

An important topic in the research of FEM is how to increase the accuracy of numerical solutions and reduce the complexity of computation. The selection of finite element basis functions will affect the accuracy of numerical solutions. In recent years, many scholars applied FEM based on spline functions to PDEs. For instance, Shi [20] combined the B-spline functions with FEM and proposed the spline finite element method to solve the equilibrium problems of the plate-beam composite elastic structures in regular regions and derived a unified computation scheme for various boundary conditions. Hughes et al. [21] put forward a new spline finite element method which applies NURBS basis functions in finite element analysis for isometric analysis. Chen et al. [22] presented spline curved surfaces based on T-meshes which can better deal with adaptive surface modeling. Peng et al. [23] developed the intrinsic extended isogeometric analysis using B-splines, in which the control points served as support points for least-squares fitting directly. Peake et al. [24] used the boundary element method based on non-uniform rational B-spline to solve the three-dimensional wave scattering problem controlled by the Helmholtz equation. Zhu et al. [25] constructed four new cubic rational Bernstein-like basis functions with two parameters by using the blossom method. These basis functions can form a normalized B-basis. Wang et al. [26] applied an integral approach to construct C-Bézier basis functions for the space $\Gamma_k = span\left\{1, t, \cdots, (t)^{k-2}, \sin(t), \cos(t)\right\}$ that extended the spaces of mixed algebra and trigonometric polynomial.

C-Bézier basis functions are one kind of spline functions that have a nonrational form and are capable of expressing circular arc and polynomial curves of high order exactly. C-Bézier basis functions also introduce the shape parameters, which increases the degree of freedom of curve construction [27]. In previous work, scholars obtained good approximate solutions by combining spline functions with the finite element. Sun et al. [28] showed that the C-Bézier and H-Bézier basis functions have a much better approximation in simulating convection-diffusion problems. In this paper, we combine the Galerkin finite element method with C-Bézier basis functions to solve unsteady elastic equations. C-Bézier basis functions are selected to construct trial and test function spaces. The numerical examples are given, and the numerical results indicate that our method has much better precision in solving unsteady elastic equations. The numerical solutions in this paper are generated in MATLAB 2018a.

The structure of this paper is as follows: In Section 2, we introduce the two-dimensional unsteady elastic equation and recall the definitions and properties of C-Bézier basis functions. In Section 3, the Galerkin finite element method is combined with C-Bézier basis functions to solve the unsteady elastic equations. In Section 4, a prior estimate for the unsteady elastic equations of the θ-difference FEM scheme is proved. In Section 5, the error estimates and corresponding convergence order under the L^∞

norm, L^2 norm and H^1 semi-norm are obtained through numerical examples, and the feasibility and effectiveness of the method is verified. In the final section, we not only summarize some comments on the overall work, but also touch upon some avenues of future research.

2. Mathematical model and C-Bézier basis

In this section, we introduce the two-dimensional unsteady elastic equation and recall the definitions and properties of C-Bézier basis functions.

2.1. Mathematical model

The initial-boundary value problem for the unsteady elastic equation is as follows, where Ω is a polygonal domain in $\mathbb{R}^2$:

$$\begin{cases} \boldsymbol{u}_{tt} - \nabla \cdot \sigma(\boldsymbol{u}) = \boldsymbol{f}, \ in\ \Omega \times [0,T], \\ \boldsymbol{u} = \boldsymbol{g}, \ on\ \partial\Omega \times [0,T], \\ \boldsymbol{u} = \boldsymbol{u}_0, \ \dfrac{\partial \boldsymbol{u}}{\partial t} = \boldsymbol{u}_{00}, \ at\ t = 0\ and\ in\ \Omega. \end{cases} \tag{2.1}$$

Let $\boldsymbol{u} = \boldsymbol{u}(x_1, x_2; t) = (u_1, u_2)^t$ be the displacement and $\boldsymbol{f} = \boldsymbol{f}(x_1, x_2; t) = (f_1, f_2)^t$ be the body force.

The stress tensor $\sigma(\boldsymbol{u})$ is defined as

$$\sigma(\boldsymbol{u}) = \begin{pmatrix} \sigma_{11}(\boldsymbol{u}) & \sigma_{12}(\boldsymbol{u}) \\ \sigma_{21}(\boldsymbol{u}) & \sigma_{22}(\boldsymbol{u}) \end{pmatrix}, \ \sigma_{ij}(\boldsymbol{u}) = \lambda(\nabla \cdot \boldsymbol{u})\delta_{ij} + 2\mu\varepsilon_{ij}(\boldsymbol{u}) \ (i,j = 1,2),$$

where λ and μ are *lamé* parameters, $\lambda \in (0, +\infty)$, $\mu \in (\mu_1, \mu_2)$, $0 < \mu_1 < \mu_2$.

The strain tensor is defined as

$$\varepsilon = \begin{pmatrix} \varepsilon_{11} & \varepsilon_{12} \\ \varepsilon_{21} & \varepsilon_{22} \end{pmatrix}, \ \varepsilon_{ij} = \frac{1}{2}\left(\frac{\partial u_i}{\partial x_j} + \frac{\partial u_j}{\partial x_i}\right).$$

2.2. C-Bézier basis functions

Definition 2.1. *The C-Bézier basis functions for the space* $\Gamma_k = span\left\{1, t, \cdots, t^{k-2}, sint, cost\right\}$ *of degrees k is defined by*

$$\begin{aligned} C_0^k(t) &= 1 - \int_0^t \delta_0^{k-1} C_0^{k-1}(s)ds, \\ C_i^k(t) &= \int_0^t \delta_{i-1}^{k-1} C_{i-1}^{k-1}(s)ds - \int_0^t \delta_i^{k-1} C_i^{k-1}(s)ds, \quad i = 1, 2, \cdots, k-1, \\ C_k^k(t) &= \int_0^t \delta_{k-1}^{k-1} C_{k-1}^{k-1}(s)ds, \end{aligned} \tag{2.2}$$

where $k \geq 2$, $t \in [0, \alpha]$, $C_0^1(t) = \frac{\sin(\alpha - t)}{\sin\alpha}$, $C_1^1(t) = \frac{\sin t}{\sin\alpha}$, $\delta_i^k = (\int_0^\alpha C_i^k(t)dt)^{-1}$ *and the shape parameter* $\alpha \in (0, \pi]$.

While $k = 2$, C-Bézier basis functions are expressed as follows:

$$\begin{aligned} C_0^2 &= \frac{1-\cos(\alpha - t)}{1-\cos\alpha}, \\ C_1^2 &= -\frac{1-\cos t+\cos\alpha-\cos(\alpha-t)}{1-\cos\alpha}, \\ C_2^2 &= \frac{1-\cos t}{1-\cos\alpha}, \end{aligned} \tag{2.3}$$

where $t \in [0, \alpha]$ and the shape parameter $\alpha \in (0, \pi]$.

In the images below, Figure 1(a) shows the quadratic C-Bézier basis function at $\alpha = \frac{\pi}{8}$ and Figure 1(b) presents the quadratic C-Bézier basis function at $\alpha = \frac{2\pi}{9}$.

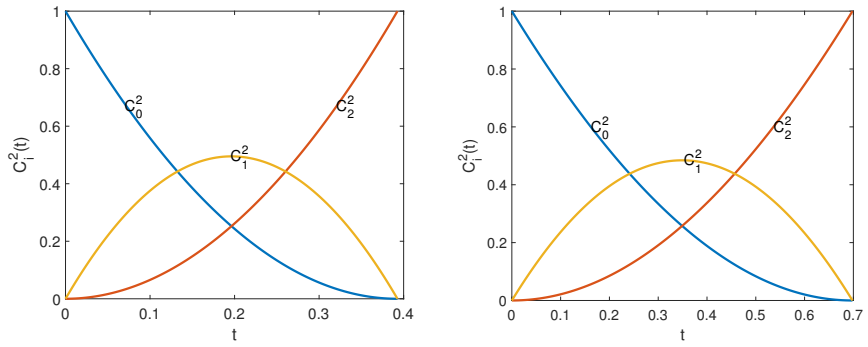

(a) $\alpha = \frac{\pi}{8}$ (b) $\alpha = \frac{2\pi}{9}$

Figure 1. C-Bézier basis functions.

We display the main properties of the C-Bézier basis here–all of these properties can be found in [26].

Property 2.1. Properties at the endpoints:

At the endpoints, the C-Bézier basis has the same properties as the Bézier basis. That is, for $k \geq 2$,

$$\begin{aligned} &C_0^k(0) = C_k^k(\alpha) = 1, \\ &[C_i^k(0)]^{(s)} = [C_i^k(\alpha)]^{(m)} = 0,\ s = 0, \cdots, i-1;\ m = 0, \cdots, n-i-1. \\ &[C_i^k(0)]^{(s)} = \delta_{s-1}^{k-1}\delta_{s-2}^{k-2}\cdots\delta_0^{k-s},\ s = 1, 2, \cdots, n. \end{aligned}$$

Property 2.2. Linear independence:

The C-Bézier basis $\left\{C_i^s(t)\right\}_{i=0}^k$ is linearly independent, and it is a basis for the space $\Gamma_k = span\left\{1, t, \cdots, t^{k-2}, sint, cost\right\}$.

Property 2.3. Positivity:

The C-Bézier basis is positive on $[0, \alpha]$ and normalized, that is,

$$\begin{aligned} &C_i^k(t) > 0, t \in [0, \alpha],\ i = 0, \cdots, k; \\ &\sum_{i=0}^{k} C_i^k(t) = 1. \end{aligned}$$

Property 2.4. Symmetry:

$$C_i^k(t) = C_{k-i}^k(\alpha - t),\ t \in [0, \alpha],\ i = 0, \cdots, k.$$

Definition 2.2. *A C-Bézier surface $S(u, v)$ of $s \times m$ degrees with control points $P_{ij}(x, y, z) \in \mathbb{R}^3$ ($i = 0, 1, \cdots, s;\ j = 0, 1, \cdots, m$) is defined as*

$$S(u, v) = \sum_{i=0}^{s} \sum_{j=0}^{m} P_{i,j} C_{i,j}^{s,m}(u, v), (u, v) \in [0, \alpha] \times [0, \beta], \tag{2.4}$$

where $C_{i,j}^{s,m}(u, v) = C_i^s(u) C_j^m(v)$ is the tensor-product C-Bézier basis. α and β are the shape parameters.

As shown in the following figure, Figure 2(a) is a biquadratic C-Bézier surface with the shape parameters $\alpha = \frac{\pi}{2}, \beta = \frac{\pi}{3}$ and the control points $P_{0,0} = (0, 0, 0)$, $P_{0,1} = (1, 0, -1)$, $P_{0,2} = (2, 0, 0)$, $P_{1,0} = (0, 2, -1)$, $P_{1,1} = (1, 2, -2)$, $P_{1,2} = (2, 2, -1)$, $P_{2,0} = (0, 4, 0)$, $P_{2,1} = (1, 4, -1)$, $P_{2,2} = (2, 4, 0)$; Figure 2(b) is a 2×3 degrees C-Bézier surface with the shape parameters $\alpha = \frac{\pi}{8}, \beta = \frac{\pi}{6}$ and the control points are $P_{0,0} = (0, 0, 1)$, $P_{0,1} = (4, 0, -2)$, $P_{0,2} = (8, 0, 2)$, $P_{0,3} = (10, 0, \frac{1}{2})$, $P_{1,0} = (0, 2, 2)$, $P_{1,1} = (4, 2, -1)$, $P_{1,2} = (8, 2, 3)$, $P_{1,3} = (10, 2, \frac{5}{2})$, $P_{2,0} = (0, 4, 1)$, $P_{2,1} = (4, 4, -2)$, $P_{2,2} = (8, 4, 2)$, $P_{2,3} = (10, 4, \frac{1}{2})$.

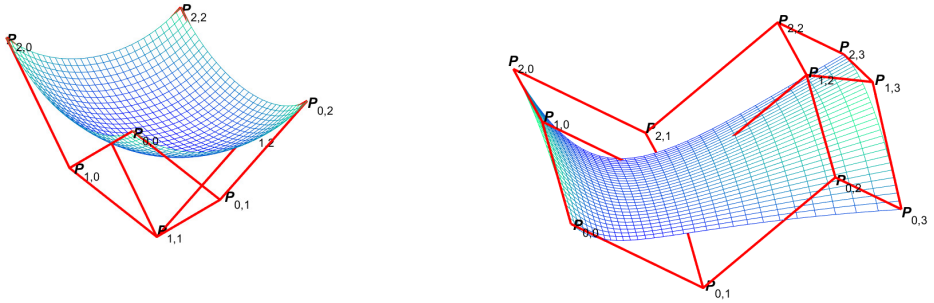

(a) 2×2 degrees C-Bézier surface (b) 2×3 degrees C-Bézier surface

Figure 2. C-Bézier surfaces.

3. C-Bézier finite element scheme

In this section, we consider combining the Galerkin finite element method with C-Bézier basis to solve the unsteady elastic equations.

As a preparation for the finite element algorithm, we briefly present the definitions of Sobolev space $H^m(\Omega)$ and corresponding norms.

Let $\Omega \in \mathbb{R}^2$ be a bounded domain. The Sobolev space $H^m(\Omega)$ is defined by

$$H^m(\Omega) = \left\{ v \in L^2(\Omega) : D^\gamma v \in L^2(\Omega),\ \text{if } |\gamma| \le m \right\},$$

with norm

$$\|v\|_{H^m(\Omega)} = \left(\sum_{|\gamma| \le m} \|D^\gamma v\|_{L^2(\Omega)}^2 \right)^{\frac{1}{2}},$$

and semi-norm

$$|v|_{H^m(\Omega)} = (\sum_{|\gamma|=m} \|D^\gamma v\|\|^2_{L^2(\Omega)})^{\frac{1}{2}}.$$

In the above formulas,

$$\gamma = (\gamma_1, \gamma_2), \quad |\gamma| = (\gamma_1 + \gamma_2), \quad D^\gamma = \frac{\partial^{|\gamma|}}{\partial^{\gamma_1}_{x_1} \partial^{\gamma_2}_{x_2}}.$$

For $m = 1$, $H^1_0(\Omega)$ is the subspace of $H^1(\Omega)$ with vanishing boundary values on $\partial\Omega$.

Based on the above definition of Sobolev space, the functional space $H^2\left(0, T; [H^1(\Omega)]^2\right)$ is defined as

$$H^2\left(0, T; [H^1(\Omega)]^2\right) = \left\{ \boldsymbol{v}(\cdot, t), \frac{\partial \boldsymbol{v}}{\partial t}(\cdot, t), \frac{\partial^2 \boldsymbol{v}}{\partial t^2} \in [H^1(\Omega)]^2, \forall t \in [0, T] \right\}. \tag{3.1}$$

3.1. Weak formulation

Now we give the weak formulation of the unsteady elastic equation in (2.1) and separate the weak formulation with Galerkin method.

Assume that $\boldsymbol{u} \in H^2\left(0, T; [H^1(\Omega)]^2\right)$, then multiplying the first equation of (2.1) by test function $\boldsymbol{v} \in \left[H^1_0(\Omega)\right]^2$ yields

$$\int_\Omega \boldsymbol{u}_{tt} \cdot \boldsymbol{v} dx_1 dx_2 - \int_\Omega (\nabla \cdot \sigma(\boldsymbol{u})) \cdot \boldsymbol{v} dx_1 dx_2 = \int_\Omega \boldsymbol{f} \cdot \boldsymbol{v}\, dx_1 dx_2,$$

then using Green formula, it's obtained as follows:

$$\int_\Omega \boldsymbol{u}_{tt} \cdot \boldsymbol{v} dx_1 dx_2 + \int_\Omega \sigma(\boldsymbol{u}) : \nabla \boldsymbol{v} dx_1 dx_2 = \int_\Omega \boldsymbol{f} \cdot \boldsymbol{v} dx_1 dx_2, \quad \forall \boldsymbol{v} \in \left[H^1_0(\Omega)\right]^2.$$

In detail, the inner product of the second-order tensor $\sigma(\boldsymbol{u}) : \nabla \boldsymbol{v}$ is given by

$$\begin{aligned}
&\sigma(\boldsymbol{u}) : \nabla \boldsymbol{v} \\
=&\begin{pmatrix} \sigma_{11}(\boldsymbol{u}) & \sigma_{12}(\boldsymbol{u}) \\ \sigma_{21}(\boldsymbol{u}) & \sigma_{22}(\boldsymbol{u}) \end{pmatrix} : \begin{pmatrix} \frac{\partial v_1}{\partial x_1} & \frac{\partial v_1}{\partial x_2} \\ \frac{\partial v_2}{\partial x_1} & \frac{\partial v_2}{\partial x_2} \end{pmatrix} \\
=&\sigma_{11}(\boldsymbol{u}) \cdot \frac{\partial v_1}{\partial x_1} + \sigma_{12}(\boldsymbol{u}) \cdot \frac{\partial v_1}{\partial x_2} + \sigma_{21}(\boldsymbol{u}) \cdot \frac{\partial v_2}{\partial x_1} + \sigma_{22}(\boldsymbol{u}) \cdot \frac{\partial v_2}{\partial x_2}.
\end{aligned}$$

Therefore, the weak formulation for the unsteady elastic equation can be obtained, finding $\boldsymbol{u} \in H^2\left(0, T; [H^1(\Omega)]^2\right)$ and

$$(\boldsymbol{u}_{tt}, \boldsymbol{v}) + a(\boldsymbol{u}, \boldsymbol{v}) = (\boldsymbol{f}, \boldsymbol{v}), \quad \forall \boldsymbol{v} \in \left[H^1_0(\Omega)\right]^2, \tag{3.2}$$

where

$$\begin{aligned}
(\boldsymbol{u}_{tt}, \boldsymbol{v}) &= \int_\Omega \boldsymbol{u}_{tt} \cdot \boldsymbol{v}\, dx_1 dx_2, \\
a(\boldsymbol{u}, \boldsymbol{v}) &= \int_\Omega \sigma(\boldsymbol{u}) : \nabla \boldsymbol{v}\, dx_1 dx_2, \\
(\boldsymbol{f}, \boldsymbol{v}) &= \int_\Omega \boldsymbol{f} \cdot \boldsymbol{v}\, dx_1 dx_2.
\end{aligned} \tag{3.3}$$

3.2. Discrete model

Taking into account the unsteady elastic equation in a rectangular domain $\Omega = [0,1] \times [0,1]$. Let Ω_h be a quasi-homogeneous rectangular mesh. The mesh size is $\boldsymbol{h} = [h_1, h_2] = \left[\frac{1}{N_1}, \frac{1}{N_2}\right]$. N_1 and N_2 represent the number of subintervals of the x-axis and y-axis of the quasi-uniform subdivision, respectively. The number of elements is $N = N_1 N_2$.

The $n_1 \times n_2$ tensor-product C-Bézier basis functions on $[0,\alpha] \times [0,\beta]$ are defined as follows:

$$C_{\bar{i},\bar{j}}^{n_1,n_2}(u,v) = C_{\bar{i}}^{n_1}(u) C_{\bar{j}}^{n_2}(v),\ \bar{i} = 0,1,\cdots,n_1;\ \bar{j} = 0,1,\cdots,n_2, \tag{3.4}$$

letting $\bar{u} = \frac{u}{\alpha}$, $\bar{v} = \frac{v}{\beta}$, where $\bar{u} \in [0,1]$, $\bar{v} \in [0,1]$. The tensor-product C-Bézier basis defined on the reference elements can be obtained:

$$C_{\bar{i},\bar{j}}^{n_1,n_2}(\bar{u},\bar{v}) = C_{\bar{i}}^{n_1}(\alpha\bar{u}) C_{\bar{j}}^{n_2}(\beta\bar{v}),\ \bar{i} = 0,\cdots,n_1;\ \bar{j} = 0,\cdots n_2. \tag{3.5}$$

Performing an affine transformation for them, let $\bar{u} = \frac{x - x_i}{h_1}$, $\bar{v} = \frac{y - y_j}{h_2}$. Therefore, the shape function on the local element can be obtained as follows:

$$C_{\bar{i},\bar{j}}^{n_1,n_2}(x,y) = C_{\bar{i}}^{n_1}(\alpha\frac{x - x_i}{h_1}) C_{\bar{j}}^{n_2}(\beta\frac{y - y_j}{h_2}),\ \bar{i} = 0,\cdots,n_1;\ \bar{j} = 0,\cdots n_2. \tag{3.6}$$

Taking into account the biquadratic C-Bézier basis on the reference rectangular element, $\hat{E} = \square\hat{A}_1\hat{A}_2\hat{A}_3\hat{A}_4$. The four vertices of the rectangle are $\hat{A}_1 = (0,0)$, $\hat{A}_2 = (1,0)$, $\hat{A}_3 = (1,1)$, $\hat{A}_4 = (0,1)$. The midpoints of the four sides $\hat{A}_1\hat{A}_2$, $\hat{A}_2\hat{A}_3$, $\hat{A}_3\hat{A}_4$ and $\hat{A}_4\hat{A}_1$ are $\hat{A}_5 = (\frac{1}{2},0)$, $\hat{A}_6 = (1,\frac{1}{2})$, $\hat{A}_7 = (\frac{1}{2},1)$ and $\hat{A}_8 = (0,\frac{1}{2})$. The center of the rectangle is $\hat{A}_9 = (\frac{1}{2},\frac{1}{2})$.

From (3.5), we derive the biquadratic tensor-product type C-Bézier basis functions on the reference element $[0,1] \times [0,1]$ as follows:

$$C_{0,0}^{2,2}(\bar{u},\bar{v}) = \frac{(1-\cos(\alpha-\alpha\bar{u}))(1-\cos(\beta-\beta\bar{v}))}{(1-\cos\alpha)(1-\cos\beta)},$$

$$C_{1,0}^{2,2}(\bar{u},\bar{v}) = -\frac{(1-\cos(\bar{u}\alpha)+\cos\alpha-\cos(\alpha-\bar{u}\alpha))(1-\cos(\beta-\beta\bar{v}))}{(1-\cos\alpha)(1-\cos\beta)},$$

$$C_{2,0}^{2,2}(\bar{u},\bar{v}) = \frac{(1-\cos(\bar{u}\alpha))(1-\cos(\beta-\beta\bar{v}))}{(1-\cos\alpha)(1-\cos\beta)},$$

$$C_{2,1}^{2,2}(\bar{u},\bar{v}) = -\frac{(1-\cos(\bar{u}\alpha))(1-\cos(\bar{v}\beta)+\cos\beta-\cos(\beta-\bar{v}\beta))}{(1-\cos\alpha)(1-\cos\beta)},$$

$$C_{2,2}^{2,2}(\bar{u},\bar{v}) = \frac{(1-\cos(\bar{u}\alpha))(1-\cos(\bar{v}\beta))}{(1-\cos\alpha)(1-\cos\beta)},$$

$$C_{1,2}^{2,2}(\bar{u},\bar{v}) = -\frac{(1-\cos(\bar{u}\alpha)+\cos\alpha-\cos(\alpha-\bar{u}\alpha))(1-\cos(\bar{v}\beta))}{(1-\cos\alpha)(1-\cos\beta)},$$

$$C_{0,2}^{2,2}(\bar{u},\bar{v}) = \frac{(1-\cos(\alpha-\alpha\bar{u}))(1-\cos(\bar{v}\beta))}{(1-\cos\alpha)(1-\cos\beta)},$$

$$C_{0,1}^{2,2}(\bar{u},\bar{v}) = \frac{(1-\cos(\alpha-\alpha\bar{u}))(1-\cos(\bar{v}\beta)+\cos\beta-\cos(\beta-\bar{v}\beta))}{(1-\cos\alpha)(1-\cos\beta)},$$

$$C_{1,1}^{2,2}(\bar{u},\bar{v}) = \frac{(1-\cos(\bar{u}\alpha)+\cos\alpha-\cos(\alpha-\bar{u}\alpha))(1-\cos(\bar{v}\beta)+\cos\beta-\cos(\beta-\bar{v}\beta))}{(1-\cos\alpha)(1-\cos\beta)},$$

where $\bar{u} \in [0,1],\ \bar{v} \in [0,1],\ \alpha \in (0,\pi],\ \beta \in (0,\pi]$.

As shown in the following figure, Figure 3 is the C-Bézier basis of the biquadratic tensor-product type on the reference element when $\alpha = \frac{\pi}{4}, \beta = \frac{\pi}{6}$.

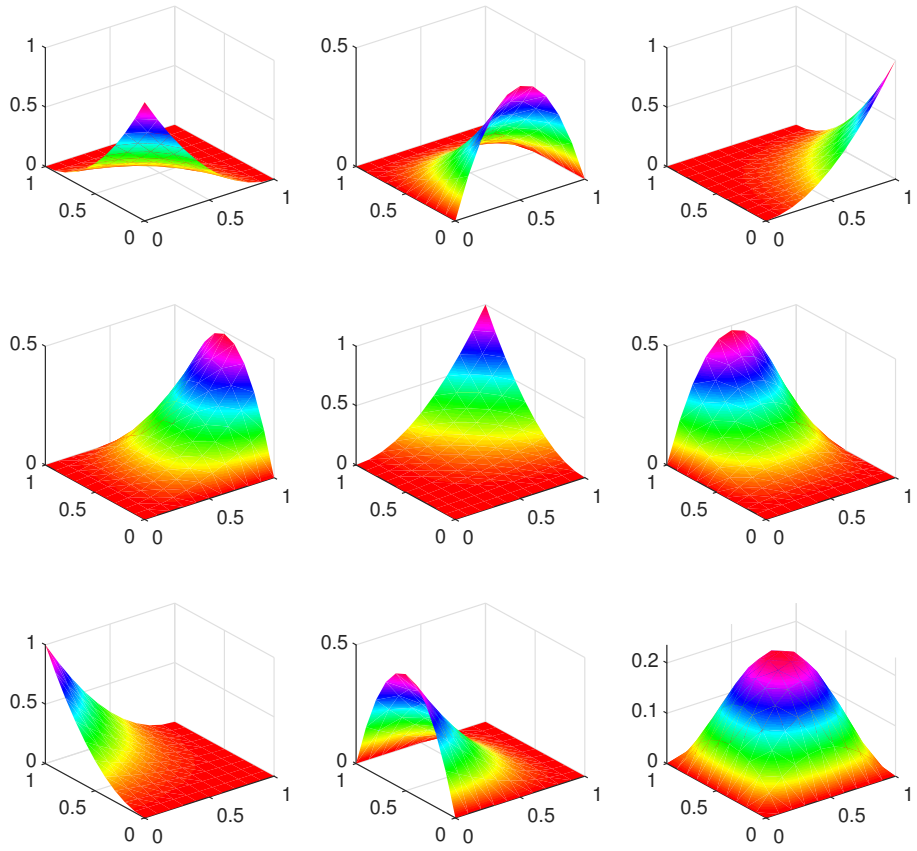

Figure 3. Biquadrate C-Bézier basis at $\alpha = \frac{\pi}{4}\ , \beta = \frac{\pi}{6}$.

Then we construct the finite element function spaces. We use the affine mapping between the general element $E = \square A_1A_2A_3A_4$ and the reference element $\hat{E} = \square \hat{A}_1\hat{A}_2\hat{A}_3\hat{A}_4$ to construct the shape functions on the local element $E_n = \square A_{1n}A_{2n}A_{3n}A_{4n}$. For $E_n \in \Omega_h$, the local finite element space is represented by $S_h(E_n)$, that is,

$$S_h(E_n) = \left\{C,\ C \in span\left\{C_{i,j}^{n_1,n_2}(x,y)\right\}_{i,j=0}^{n_1,n_2}, \forall (x,y) \in E_n\right\}. \tag{3.7}$$

We concatenate the local finite element spaces on all elements to construct a finite dimensional subspace. The finite element space is

$$U_h(n_1,n_2) = \{C,\ C \in S_h(E_n), \forall E_n \in \Omega_h\}. \tag{3.8}$$

U_{h0} denotes a compactly supported function space with zero on the boundary of U_h as follows:

$$U_{h0}(n_1,n_2) = \{C \in U_h,\ C|_{\partial\Omega} = 0,\ \forall\ E_n \in \Omega_h\}. \tag{3.9}$$

Subsequently, the Galerkin formulation of the unsteady elastic equation is to find $\boldsymbol{u}_h \in H^2\left(0,T;[U_h]^2\right)$, such that

$$(\boldsymbol{u}_{h_{tt}},\boldsymbol{v}_h)+a(\boldsymbol{u}_h,\boldsymbol{v}_h)=(\boldsymbol{f},\boldsymbol{v}_h),\ \ \forall \boldsymbol{v}_h\in[U_{h0}]^2\,, \tag{3.10}$$

where

$$\begin{aligned}(\boldsymbol{u}_{h_{tt}},\boldsymbol{v}_h)&=\int_\Omega \boldsymbol{u}_{h_{tt}}\cdot\boldsymbol{v}_h\,dx_1dx_2,\\ a(\boldsymbol{u}_h,\boldsymbol{v}_h)&=\int_\Omega \sigma(\boldsymbol{u}_h):\nabla\boldsymbol{v}_h dx_1dx_2,\\ (\boldsymbol{f},\boldsymbol{v}_h)&=\int_\Omega \boldsymbol{f}\cdot\boldsymbol{v}_h dx_1dx_2.\end{aligned} \tag{3.11}$$

The dimension of finite element space U_h introduced in (3.8) and the number of global basis functions are $N_b=(2N_1+1)(2N_2+1)$. Let C_j $(j=1,\cdots,N_b)$ denote the global finite element basis functions of finite element space U_h, so that $U_h=\text{span}\left\{C_j\right\}_{j=1}^{N_b}$ and the finite element numerical solution vector is

$$\boldsymbol{u}_h=(u_{1h},u_{2h})^t,$$

where

$$u_{1h}=\sum_{j=1}^{N_b}u_{1j}(t)C_j\ ,\ u_{2h}=\sum_{j=1}^{N_b}u_{2j}(t)C_j.$$

Then we set up a linear algebraic system for $u_{1j}(t)$ and $u_{2j}(t)$ $(j=1,\cdots,N_b)$, and solve it to obtain the finite element solution $\boldsymbol{u}_h=(u_{1h},u_{2h})^t$. We choose $\boldsymbol{v}_h=(C_i,0)^t$ $(i=1,\cdots,N_b)$ and $\boldsymbol{v}_h=(0,C_i)^t$ $(i=1,\cdots,N_b)$ in the Galerkin formulation. That is, in the first set of test functions, we choose $v_{1h}=C_i$ $(i=1,\cdots,N_b)$ and $v_{2h}=0$; in the second set of test functions, we choose $v_{1h}=0$ and $v_{2h}=C_i$ $(i=1,\cdots,N_b)$. Then, we obtain two sets of equations:

$$\begin{aligned}&\sum_{j=1}^{N_b}u_{1j}''(t)\int_\Omega C_jC_i dx_1dx_2\\ &+\sum_{j=1}^{N_b}u_{1j}\left(\int_\Omega\lambda\frac{\partial C_j}{\partial x_1}\frac{\partial C_i}{\partial x_1}dx_1dx_2+2\int_\Omega\mu\frac{\partial C_j}{\partial x_1}\frac{\partial C_i}{\partial x_1}dx_1dx_2+\int_\Omega\mu\frac{\partial C_j}{\partial x_2}\frac{\partial C_i}{\partial x_2}dx_1dx_2\right)\\ &+\sum_{j=1}^{N_b}u_{2j}\left(\int_\Omega\lambda\frac{\partial C_j}{\partial x_2}\frac{\partial C_i}{\partial x_1}dx_1dx_2+\int_\Omega\mu\frac{\partial C_j}{\partial x_1}\frac{\partial C_i}{\partial x_2}dx_1dx_2\right)\\ =&\int_\Omega f_1C_i dx_1dx_2,\\ &\sum_{j=1}^{N_b}u_{2j}''(t)\int_\Omega C_jC_i dx_1dx_2+\sum_{j=1}^{N_b}u_{1j}\left(\int_\Omega\lambda\frac{\partial C_j}{\partial x_1}\frac{\partial C_i}{\partial x_2}dx_1dx_2+\int_\Omega\mu\frac{\partial C_j}{\partial x_2}\frac{\partial C_i}{\partial x_1}dx_1dx_2\right)\\ &\sum_{j=1}^{N_b}u_{2j}\left(\int_\Omega\lambda\frac{\partial C_j}{\partial x_2}\frac{\partial C_i}{\partial x_2}dx_1dx_2+2\int_\Omega\mu\frac{\partial C_j}{\partial x_2}\frac{\partial C_i}{\partial x_2}dx_1dx_2+\int_\Omega\mu\frac{\partial C_j}{\partial x_1}\frac{\partial C_i}{\partial x_1}dx_1dx_2\right)\\ =&\int_\Omega f_2C_i dx_1dx_2.\end{aligned}$$

Define the stiffness matrix

$$A = \begin{pmatrix} A_1 + 2A_2 + A_3 & A_4 + A_5 \\ A_6 + A_7 & A_8 + 2A_3 + A_2 \end{pmatrix},$$

where

$$A_1 = \left[\int_\Omega \lambda \frac{\partial C_j}{\partial x_1}\frac{\partial C_i}{\partial x_1} dx_1 dx_2\right]_{i,j=1}^{N_b}, \; A_2 = \left[\int_\Omega \mu \frac{\partial C_j}{\partial x_1}\frac{\partial C_i}{\partial x_1} dx_1 dx_2\right]_{i,j=1}^{N_b},$$
$$A_3 = \left[\int_\Omega \mu \frac{\partial C_j}{\partial x_2}\frac{\partial C_i}{\partial x_2} dx_1 dx_2\right]_{i,j=1}^{N_b}, \; A_4 = \left[\int_\Omega \lambda \frac{\partial C_j}{\partial x_2}\frac{\partial C_i}{\partial x_1} dx_1 dx_2\right]_{i,j=1}^{N_b},$$
$$A_5 = \left[\int_\Omega \mu \frac{\partial C_j}{\partial x_1}\frac{\partial C_i}{\partial x_2} dx_1 dx_2\right]_{i,j=1}^{N_b}, \; A_6 = \left[\int_\Omega \lambda \frac{\partial C_j}{\partial x_1}\frac{\partial C_i}{\partial x_2} dx_1 dx_2\right]_{i,j=1}^{N_b},$$
$$A_7 = \left[\int_\Omega \mu \frac{\partial C_j}{\partial x_2}\frac{\partial C_i}{\partial x_1} dx_1 dx_2\right]_{i,j=1}^{N_b}, \; A_8 = \left[\int_\Omega \lambda \frac{\partial C_j}{\partial x_2}\frac{\partial C_i}{\partial x_2} dx_1 dx_2\right]_{i,j=1}^{N_b}.$$

Define the block mass matrix

$$M = \begin{pmatrix} M_e & \mathbb{O}_4 \\ \mathbb{O}_4 & M_e \end{pmatrix},$$

where

$$M_e = [m_{i,j}]_{i,j=1}^{N_b} = \left[\int_\Omega C_j C_i dx\right]_{i,j=1}^{N_b}, \quad \mathbb{O}_4 = [0_{i,j}]_{i,j=1}^{N_b}.$$

Define the load vector

$$\vec{b} = (\vec{b}_1, \vec{b}_2)^t,$$

where

$$\vec{b}_1 = \left[\int_\Omega f_1 C_i dx_1 dx_2\right]_{i=1}^{N_b}, \quad \vec{b}_2 = \left[\int_\Omega f_2 C_i dx_1 dx_2\right]_{i=1}^{N_b}.$$

Define the unknown vector

$$\vec{X} = (\vec{X}_1, \vec{X}_2)^t,$$

where

$$\vec{X}_1 = [u_{1j}]_{j=1}^{N_b}, \; \vec{X}_2 = [u_{2j}]_{j=1}^{N_b}.$$

Then, we get a system of ordinary differential equations for $u_{1j}(t)$ and $u_{2j}(t)$ $(j = 1, \cdots, N_b)$

$$M\vec{X}''(t) + A(t)\vec{X}(t) = \vec{b}(t). \tag{3.12}$$

So far, we gain a semi-discretization Galerkin function (3.12).

If we further discretize the space-time domain $[0, T]$, let $0 = t_0 < t_1 < \cdots < t_{M_m} = T$, the time step is τ, $t_m = m\tau$, $m = 1, 2, \cdots, M_m$ and assume $\vec{X}^m$ is the numerical solution of $\vec{X}(t_m)$, the corresponding θ-scheme finite difference is

$$M\frac{\vec{X}^{m+1} - 2\vec{X}^m + \vec{X}^{m-1}}{\tau^2} + A\vec{X}^{m+\theta} = \vec{b}^m, \tag{3.13}$$

when using the notations $\vec{X}^{m+\theta} = \theta\vec{X}^{m+1} + (1-2\theta)\vec{X}^{m} + \theta\vec{X}^{m-1}$, $\vec{b}^{m} = \vec{b}(t_m)$. Let $\tilde{A} = \frac{M}{\tau^2} + \theta A$, $\tilde{\vec{b}} = \vec{b}^{m} + [\frac{2M}{\tau^2} - (1-2\theta)A]\vec{X}^{m} - [\frac{M}{\tau^2} + \theta A]\vec{X}^{m-1}$ and then substituting (3.13) can obtain a fully discrete algebraic system related to time,

$$\tilde{A}\vec{X}^{m+1} = \tilde{\vec{b}}, \tag{3.14}$$

so we can solve the system (3.14) and obtain the unknown vector group $\vec{X}^{m+1}$.

Here, θ is the parameter of the specific scheme of the time discrete layer, and different values correspond to different difference schemes. When $\theta = 0$, it is an explicit scheme with poor stability; when $\theta = 0.25$, it is an implicit format with better stability, and it is also a format with more practical applications.

4. A prior estimate

For simplicity, we consider a uniform grid in $[0, T]$, with step $\tau > 0$. Let $\vec{X}^{m} = \vec{X}(x_1, x_2; t_m)$, $0 = t_0 < t_1 < \cdots < t_{M_m} = T$, $t_m = m\tau, m = 1, 2, \cdots, M_m$. As a basic scheme for the numerical solution of the problem (2.1) we will use a three-level scheme with weight ($\theta = const$):

$$M\frac{\vec{X}^{m+1} - 2\vec{X}^{m} + \vec{X}^{m-1}}{\tau^2} + A[\theta\vec{X}^{m+1} + (1-2\theta)\vec{X}^{m} + \theta\vec{X}^{m-1}] = \vec{b}^{m},\ m = 1, 2, \cdots, M_m. \tag{4.1}$$

Give the initial conditions, we put $\vec{X}^{0} = \vec{X}(x_1, x_2; 0)$, $\vec{X}^{1} = \frac{\partial\vec{X}(x_1,x_2;0)}{\partial t}$.

Let us derive a stability estimate with respect to the initial data and right-hand side, for the standard scheme with weights (4.1).

Theorem 4.1. If $\theta \geq 0.25$, the following a priori estimate for the solution of (4.1) holds:

$$\left\|\vec{X}^{m+1}\right\|_{*} \leq \left\|\vec{X}^{m}\right\|_{*} + \tau\left\|\vec{b}^{m}\right\|, \tag{4.2}$$

where now

$$\left\|\vec{X}^{m+1}\right\|_{*}^{2} = \left\|\frac{\vec{X}^{m+1} - \vec{X}^{m}}{\tau}\right\|_{ME+(\theta-\frac{1}{4})\tau^2 A}^{2} + \left\|\frac{\vec{X}^{m+1} + \vec{X}^{m}}{2}\right\|_{A}^{2} \tag{4.3}$$

is the discrete time analog of $\left\|\vec{X}\right\|_{*}^{2}$. Here, E denotes the identity operator.

Proof. Given the equality

$$\theta\vec{X}^{m+1} + (1-2\theta)\vec{X}^{m} + \theta\vec{X}^{m-1} = \frac{1}{4}(\vec{X}^{m+1} + 2\vec{X}^{m} + \vec{X}^{m-1}) + (\theta - \frac{1}{4})(\vec{X}^{m+1} - 2\vec{X}^{m} + \vec{X}^{m-1}),$$

we write (4.1) as

$$D\frac{\vec{X}^{m+1} - 2\vec{X}^{m} + \vec{X}^{m-1}}{\tau^2} + A\frac{\vec{X}^{m+1} + 2\vec{X}^{m} + \vec{X}^{m-1}}{4} = \vec{b}^{m}, \tag{4.4}$$

where

$$D = ME + (\theta - \frac{1}{4})\tau^2 A.$$

Let us introduce two new grid functions:

$$\vec{V}^{m} = \frac{\vec{X}^{m} + \vec{X}^{m-1}}{2},\ \ \vec{W}^{m} = \frac{\vec{X}^{m} - \vec{X}^{m-1}}{\tau},$$

and from (4.4) we arrive at the equation

$$D\frac{\vec{W}^{m+1}+\vec{W}^{m}}{\tau}+A\frac{\vec{V}^{m+1}+\vec{V}^{m}}{2}=\vec{b}^{m}. \tag{4.5}$$

Scalarly multiplying both sides of (4.5) by $\tau(\vec{W}^{m+1}+\vec{W}^{m})=2(\vec{V}^{m+1}-\vec{V}^{m})$, we get the equality

$$\left\|\vec{W}^{m+1}\right\|_{D}^{2}-\left\|\vec{W}^{m}\right\|_{D}^{2}+\left\|\vec{V}^{m+1}\right\|_{A}^{2}-\left\|\vec{V}^{m}\right\|_{A}^{2}=\tau(\vec{b}^{m},\vec{W}^{m+1}+\vec{W}^{m}).$$

In the left-hand side of this equality, we have

$$\left\|\vec{W}^{m+1}\right\|_{D}^{2}-\left\|\vec{W}^{m}\right\|_{D}^{2}+\left\|\vec{V}^{m+1}\right\|_{A}^{2}-\left\|\vec{V}^{m}\right\|_{A}^{2}=\left\|\vec{X}^{m+1}\right\|_{*}^{2}-\left\|\vec{X}^{m}\right\|_{*}^{2},$$

and for the right-hand side, we use the estimate as follows:

$$(\vec{b}^{m},\vec{W}^{m+1}+\vec{W}^{m})\leq\left\|\vec{b}^{m}\right\|\left\|\vec{W}^{m+1}+\vec{W}^{m}\right\|\leq\left\|\vec{b}^{m}\right\|(\left\|\vec{X}^{m+1}\right\|_{*}+\left\|\vec{X}^{m}\right\|_{*}),$$

then, we obtain the prior estimate (4.2).

5. Numerical examples

In this section, several examples are presented to verify the feasibility and effectiveness of our method. The approximate solutions are solved by MATLAB software, and the errors and convergence order between the exact solutions and the finite element solutions under the L^{∞} norm, L^{2} norm and H^{1} semi-norm are obtained by numerical experiments. We use biquadratic basis functions to construct the trial and test function spaces of the finite element method, and the finite element nodes and the grids are the same. In the finite difference scheme of time processing, θ-scheme is used to solve the fully discrete system (3.14), and finally the numerical solution $\boldsymbol{u}_h$ is obtained. Compared with Lagrange finite element scheme, numerical accuracy is improved by 1–3 orders of magnitude and the method proposed possesses a rapid convergence rate when we use C-Bézier basis functions, which implies that the C-Bézier finite element scheme has a much better approximation in simulating unsteady elastic equations.

The errors for the finite element method shall be measured in three norms defined as follows:

L^{∞} norm error:

$$\|\boldsymbol{u}-\boldsymbol{u}_h\|_{\infty}=max\left(\|u_1-u_{1h}\|_{\infty},\|u_2-u_{2h}\|_{\infty}\right),$$

where

$$\|u_1-u_{1h}\|_{\infty}=sup\,|u_1-u_{1h}|,$$
$$\|u_2-u_{2h}\|_{\infty}=sup\,|u_2-u_{2h}|.$$

L^{2} norm error:

$$\|\boldsymbol{u}-\boldsymbol{u}_h\|_{0}=\sqrt{\|u_1-u_{1h}\|_{0}^{2}+\|u_2-u_{2h}\|_{0}^{2}},$$

where

$$\|u_1-u_{1h}\|_{0}=\sqrt{\int_{\Omega}(u_1-u_{1h})^{2}\;dx_1dx_2},$$

$$\|u_2-u_{2h}\|_{0}=\sqrt{\int_{\Omega}(u_2-u_{2h})^{2}\;dx_1dx_2}.$$

H^1 semi-norm error:

$$|\boldsymbol{u} - \boldsymbol{u}_h|_1 = \sqrt{|u_1 - u_{1h}|_1^2 + |u_2 - u_{2h}|_1^2},$$

where

$$|u_1 - u_{1h}|_1 = \sqrt{\int_\Omega \left(\left(\frac{\partial(u_1 - u_{1h})}{\partial x_1} \right)^2 + \left(\frac{\partial(u_1 - u_{1h})}{\partial x_2} \right)^2 \right) dx_1 dx_2},$$

$$|u_2 - u_{2h}|_1 = \sqrt{\int_\Omega \left(\left(\frac{\partial(u_2 - u_{2h})}{\partial x_1} \right)^2 + \left(\frac{\partial(u_2 - u_{2h})}{\partial x_2} \right)^2 \right) dx_1 dx_2}.$$

Then, the convergence order of the three norms is calculated by using the error norm values corresponding to the coarse grid E_N and the fine grid E_{2N} formed by the upper and lower spatial subdivisions,

$$r = \frac{ln(E_N) - ln(E_{2N})}{ln(2)}. \tag{5.1}$$

Then the stability and convergence speed of the numerical method are verified according to the convergence order.

Example 5.1. Consider following two-dimensional unsteady elastic equation in a rectangular domain with Dirichlet condition and the *lamé* parameter $\lambda = 2, \mu = 1$, where $\Omega = [0, 1] \times [0, 1]$,

$$\begin{cases} \boldsymbol{u}_{tt} - \nabla \cdot \sigma(\boldsymbol{u}) = \boldsymbol{f}(x, y; t), \ in\ \Omega \times [0, 1], \\ \boldsymbol{u} = (0, 0)^t, \ on\ \partial\Omega \times [0, 1], \\ \boldsymbol{u}_0 = (0, 0)^t, \ \boldsymbol{u}_{00} = (0, 0)^t, \ at\ t = 0\ and\ in\ \Omega. \end{cases}$$

The displacement $\boldsymbol{u} = \boldsymbol{u}(x, y; t) = (u_1, u_2)^t$ is

$$u_1 = t^2 sin(\pi x) sin(\pi y), \ u_2 = t^2 sin(\pi x) sin(\pi y),$$

and the body force $\boldsymbol{f}(x, y; t) = (f_1, f_2)^t$ is

$$f_1 = [2 + (\lambda + 3\mu)t^2] sin(\pi x) sin(\pi y) - (\lambda + \mu) t^2 \pi^2 cos(\pi x) cos(\pi y),$$
$$f_2 = [2 + (\lambda + 3\mu)t^2] sin(\pi x) sin(\pi y) - (\lambda + \mu) t^2 \pi^2 cos(\pi x) cos(\pi y).$$

Here, we take the time step $\tau = (\frac{h_1 + h_2}{2})^2$, combine with $\theta = 0.25$ and $\theta = 1$, then we calculate the three error norms and the corresponding convergence order between the numerical solution and the true solution. The numerical errors of $\theta = 0.25$ and $\theta = 1$ at the Gauss points are shown in Tables 1 and 2, and the corresponding convergence orders are shown in Tables 3 and 4, respectively. The error comparison graphs under the two difference schemes of C-Bézier and Lagrange basis functions are shown in Figures 4 and 5.

Table 1. The numerical errors with $\theta = 0.25$ at $t = 1$ on Gauss points.

Basis	(h_1, h_2)	(α, β)	$\|u - u_h\|_\infty$	$\|u - u_h\|_0$	$\|u - u_h\|_1$
Lagrange	$(\frac{1}{2}, \frac{1}{2})$	-	$2.7300e-02$	$1.9000e-02$	$2.9040e-01$
	$(\frac{1}{4}, \frac{1}{4})$	-	$3.6000e-03$	$2.4000e-03$	$7.2900e-02$
	$(\frac{1}{8}, \frac{1}{8})$	-	$4.3043e-04$	$2.9490e-04$	$1.8100e-02$
	$(\frac{1}{16}, \frac{1}{16})$	-	$5.1902e-05$	$3.6546e-05$	$4.5000e-03$
C-Bézier	$(\frac{1}{2}, \frac{1}{2})$	$(\frac{\pi}{2}, \frac{\pi}{2})$	$1.1600e-03$	$1.1000e-03$	$1.0500e-02$
	$(\frac{1}{4}, \frac{1}{4})$	$(\frac{\pi}{4}, \frac{\pi}{4})$	$6.4629e-05$	$3.7382e-05$	$2.2604e-04$
	$(\frac{1}{8}, \frac{1}{8})$	$(\frac{\pi}{8}, \frac{\pi}{8})$	$2.0840e-06$	$1.1235e-06$	$8.3533e-06$
	$(\frac{1}{16}, \frac{1}{16})$	$(\frac{\pi}{16}, \frac{\pi}{16})$	$8.4527e-08$	$4.6837e-08$	$3.1371e-07$

Table 2. The numerical errors with $\theta = 1$ at $t = 1$ on Gauss points.

Basis	(h_1, h_2)	(α, β)	$\|u - u_h\|_\infty$	$\|u - u_h\|_0$	$\|u - u_h\|_1$
Lagrange	$(\frac{1}{2}, \frac{1}{2})$	-	$2.7200e-02$	$1.9000e-02$	$2.9000e-01$
	$(\frac{1}{4}, \frac{1}{4})$	-	$3.6000e-03$	$2.4000e-03$	$7.2900e-02$
	$(\frac{1}{8}, \frac{1}{8})$	-	$4.3046e-04$	$2.9492e-04$	$1.8100e-02$
	$(\frac{1}{16}, \frac{1}{16})$	-	$5.1904e-05$	$3.6546e-05$	$4.5000e-03$
C-Bézier	$(\frac{1}{2}, \frac{1}{2})$	$(\frac{\pi}{2}, \frac{\pi}{2})$	$1.2000e-03$	$1.1003e-03$	$1.0007e-02$
	$(\frac{1}{4}, \frac{1}{4})$	$(\frac{\pi}{4}, \frac{\pi}{4})$	$6.7056e-05$	$3.7072e-05$	$2.6707e-04$
	$(\frac{1}{8}, \frac{1}{8})$	$(\frac{\pi}{8}, \frac{\pi}{8})$	$3.9330e-06$	$2.2028e-06$	$1.2577e-05$
	$(\frac{1}{16}, \frac{1}{16})$	$(\frac{\pi}{16}, \frac{\pi}{16})$	$2.5268e-07$	$1.3948e-07$	$8.3322e-07$

Table 3. Convergence order under the three norms with $\theta = 0.25$ at $t = 1$.

Basis	(h_1, h_2)	(α, β)	L^∞-order	L^2-order	H^1-order
Lagrange	$(\frac{1}{2}, \frac{1}{2})$	-	-	-	-
	$(\frac{1}{4}, \frac{1}{4})$	-	2.9228	2.9849	1.9941
	$(\frac{1}{8}, \frac{1}{8})$	-	3.0641	3.0247	2.0100
	$(\frac{1}{16}, \frac{1}{16})$	-	3.0519	3.0124	2.0080
C-Bézier	$(\frac{1}{2}, \frac{1}{2})$	$(\frac{\pi}{2}, \frac{\pi}{2})$	-	-	-
	$(\frac{1}{4}, \frac{1}{4})$	$(\frac{\pi}{4}, \frac{\pi}{4})$	4.1615	4.8914	5.2267
	$(\frac{1}{8}, \frac{1}{8})$	$(\frac{\pi}{8}, \frac{\pi}{8})$	4.0917	4.0695	4.4107
	$(\frac{1}{16}, \frac{1}{16})$	$(\frac{\pi}{16}, \frac{\pi}{16})$	3.9605	3.9846	3.9137

Table 4. Convergence order under the three norms with $\theta = 1$ at $t = 1$.

Basis	(h_1, h_2)	(α, β)	L^∞-order	L^2-order	H^1-order
Lagrange	$(\frac{1}{2}, \frac{1}{2})$	-	-	-	-
	$(\frac{1}{4}, \frac{1}{4})$	-	2.9175	2.9849	1.9941
	$(\frac{1}{8}, \frac{1}{8})$	-	3.0640	3.0246	2.0100
	$(\frac{1}{16}, \frac{1}{16})$	-	3.0520	3.0124	2.0080
C-Bézier	$(\frac{1}{2}, \frac{1}{2})$	$(\frac{\pi}{2}, \frac{\pi}{2})$	-	-	-
	$(\frac{1}{4}, \frac{1}{4})$	$(\frac{\pi}{4}, \frac{\pi}{4})$	4.1658	4.8790	5.3346
	$(\frac{1}{8}, \frac{1}{8})$	$(\frac{\pi}{8}, \frac{\pi}{8})$	4.9548	5.0562	4.7580
	$(\frac{1}{16}, \frac{1}{16})$	$(\frac{\pi}{16}, \frac{\pi}{16})$	4.6238	4.5842	4.7348

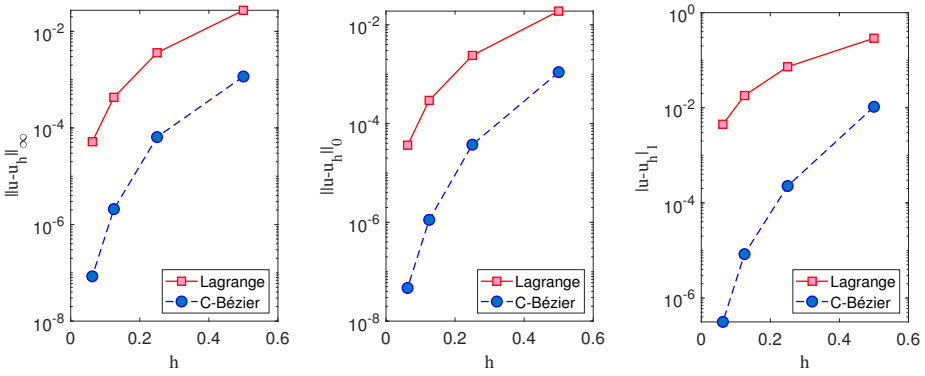

(a) $\|\boldsymbol{u} - \boldsymbol{u}_h\|_\infty$ (b) $\|\boldsymbol{u} - \boldsymbol{u}_h\|_0$ (c) $|\boldsymbol{u} - \boldsymbol{u}_h|_1$

Figure 4. The error comparison with $\theta = 0.25$ at $t = 1$.

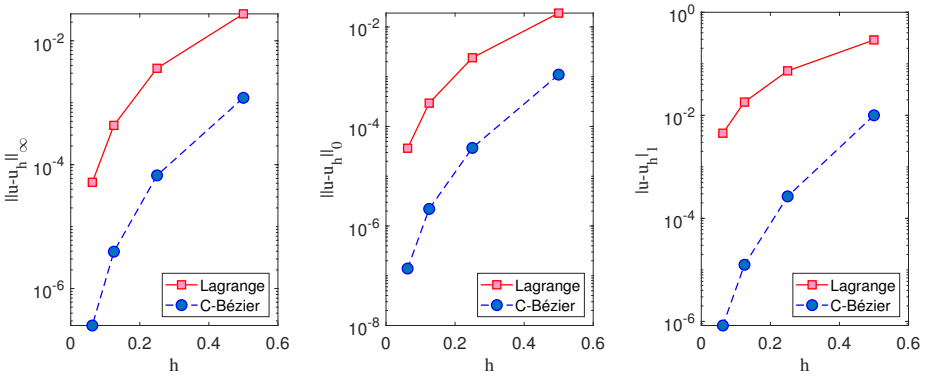

(a) $\|\boldsymbol{u} - \boldsymbol{u}_h\|_\infty$ (b) $\|\boldsymbol{u} - \boldsymbol{u}_h\|_0$ (c) $|\boldsymbol{u} - \boldsymbol{u}_h|_1$

Figure 5. The error comparison with $\theta = 1$ at $t = 1$.

It is observed that the numerical solutions derived by the C-Bézier basis is 1–3 orders of magnitude higher than that of Lagrange basis under the θ difference scheme, and the C-Bézier finite element

method has 4-order convergence in the L^∞ norm, L^2 norm and H^1 semi-norm. This indicates that the C-Bézier finite element method works well for unsteady elastic equations involving Dirichlet boundary conditions.

Example 5.2. Consider the following two-dimensional pure displacement problem of the unstady elastic equation under homogeneous boundary conditions and the *lamé* parameter $\lambda = 3$, $\mu = 5$, where $\Omega = [0, 1] \times [0, 1]$,

$$\begin{cases} \boldsymbol{u}_{tt} - \nabla \cdot \sigma(\boldsymbol{u}) = \boldsymbol{f}(x, y; t), \ in\ \Omega \times [0, 1], \\ \boldsymbol{u} = (0, 0)^t, \ on\ \partial\Omega \times [0, 1], \\ \boldsymbol{u}_0(x, y) = (0, 0)^t, \boldsymbol{u}_{00}(x, y) = (0, -y(y-1)sin(\pi x)sin(\pi y))^t, \end{cases}$$

where the exact solution $\boldsymbol{u} = \boldsymbol{u}(x, y; t) = (u_1, u_2)^t$ is

$$u_1 = t(t-1)y(y-1)sin(\pi x)sin(\pi y), u_2 = \pi t^2 x(x-1)sin(\pi x)sin(\pi y),$$

and the body force $\boldsymbol{f}(x, y; t) = (f_1, f_2)^t$ is

$$\begin{aligned} f_1 =& 2y(y-1)sin(\pi x)sin(\pi y) + (\lambda + 2\mu)\pi^2 t(t-1)y(y-1)sin(\pi x)sin(\pi y) \\ & - (\lambda + \mu)\pi^2 t^2 cos(\pi y)[(2x-1)sin(\pi x) + \pi x(x-1)cos(\pi x)] \\ & - \mu t(t-1)sin(\pi x)[2sin(\pi y) + 2\pi(2y-1)cos(\pi y) - \pi^2 y(y-1)sin(\pi y)]; \\ f_2 =& 2\pi x(x-1)sin(\pi x)sin(\pi y) - \pi(\lambda + \mu)t(t-1)cos(\pi x)[(2y-1)sin(\pi y) \\ & + \pi y(y-1)cos(\pi y)] - \pi\mu t^2 sin(\pi y)[2sin(\pi x) + 2\pi(2x-1)cos(\pi x) \\ & - \pi^2 x(x-1)sin(\pi x)] + \pi^3(\lambda + 2\mu)t^2 x(x-1)sin(\pi x)sin(\pi y). \end{aligned}$$

We take the time step $\tau = (\frac{h_1+h_2}{2})^2$, the numerical errors of $\theta = 0.25$ and $\theta = 1$ at the Gauss points are shown in Tables 5 and 6, and the corresponding convergence orders are shown in Tables 7 and 8, respectively. Figures 6 and 7 compare the errors of C-Bézier and Lagrange basis functions for the two difference schemes under $\|u - u_h\|_\infty$, $\|u - u_h\|_0$ and $|u - u_h|_1$.

Table 5. The numerical errors with $\theta = 0.25$ at $t = 1$ on Gauss points.

Basis	(h_1, h_2)	(α, β)	$\|u - u_h\|_\infty$	$\|u - u_h\|_0$	$\|u - u_h\|_1$
Lagrange	$(\frac{1}{2}, \frac{1}{2})$	-	$6.4900e-02$	$3.0800e-02$	$5.8300e-01$
	$(\frac{1}{4}, \frac{1}{4})$	-	$8.9000e-03$	$3.9000e-03$	$1.2400e-01$
	$(\frac{1}{8}, \frac{1}{8})$	-	$1.2000e-03$	$4.9088e-04$	$3.0600e-02$
	$(\frac{1}{16}, \frac{1}{16})$	-	$1.4766e-04$	$6.1519e-05$	$7.6000e-03$
C-Bézier	$(\frac{1}{2}, \frac{1}{2})$	$(\frac{5\pi}{6}, \frac{\pi}{2})$	$8.7000e-03$	$4.3000e-03$	$4.5900e-02$
	$(\frac{1}{4}, \frac{1}{4})$	$(\frac{\pi}{2}, \frac{\pi}{4})$	$8.4000e-04$	$4.7055e-04$	$1.0200e-02$
	$(\frac{1}{8}, \frac{1}{8})$	$(\frac{\pi}{4}, \frac{\pi}{8})$	$8.0392e-05$	$5.3915e-05$	$2.1000e-03$
	$(\frac{1}{16}, \frac{1}{16})$	$(\frac{\pi}{8}, \frac{\pi}{16})$	$7.7466e-06$	$6.2311e-06$	$5.1000e-04$

Table 6. The numerical errors with $\theta = 1$ at $t = 1$ on Gauss points.

Basis	(h_1, h_2)	(α, β)	$\|\|u - u_h\|\|_\infty$	$\|\|u - u_h\|\|_0$	$\|u - u_h\|_1$
Lagrange	$(\frac{1}{2}, \frac{1}{2})$	-	$6.5300e-02$	$3.0700e-02$	$5.5750e-01$
	$(\frac{1}{4}, \frac{1}{4})$	-	$8.9000e-03$	$3.9000e-03$	$1.2390e-01$
	$(\frac{1}{8}, \frac{1}{8})$	-	$1.2000e-03$	$4.9092e-04$	$3.0600e-02$
	$(\frac{1}{16}, \frac{1}{16})$	-	$1.4754e-04$	$6.1522e-05$	$7.6000e-03$
C-Bézier	$(\frac{1}{2}, \frac{1}{2})$	$(\frac{5\pi}{6}, \frac{\pi}{2})$	$8.9760e-03$	$6.6711e-03$	$6.2550e-02$
	$(\frac{1}{4}, \frac{1}{4})$	$(\frac{\pi}{2}, \frac{\pi}{4})$	$9.1761e-04$	$7.6076e-04$	$1.5600e-02$
	$(\frac{1}{8}, \frac{1}{8})$	$(\frac{\pi}{4}, \frac{\pi}{8})$	$8.5430e-05$	$7.6793e-05$	$3.1000e-03$
	$(\frac{1}{16}, \frac{1}{16})$	$(\frac{\pi}{8}, \frac{\pi}{16})$	$8.6433e-06$	$7.9016e-06$	$6.1891e-04$

Table 7. Convergence order under the three norms with $\theta = 0.25$ at $t = 1$.

Basis	(h_1, h_2)	(α, β)	L^∞-order	L^2-order	H^1-order
Lagrange	$(\frac{1}{2}, \frac{1}{2})$	-	-	-	-
	$(\frac{1}{4}, \frac{1}{4})$	-	2.87523	2.9767	2.1698
	$(\frac{1}{8}, \frac{1}{8})$	-	2.8908	2.9899	2.0176
	$(\frac{1}{16}, \frac{1}{16})$	-	3.0200	2.9963	2.0095
C-Bézier	$(\frac{1}{2}, \frac{1}{2})$	$(\frac{5\pi}{6}, \frac{\pi}{2})$	-	-	-
	$(\frac{1}{4}, \frac{1}{4})$	$(\frac{\pi}{2}, \frac{\pi}{4})$	3.2901	3.1324	2.0035
	$(\frac{1}{8}, \frac{1}{8})$	$(\frac{\pi}{4}, \frac{\pi}{8})$	3.4251	3.3083	2.3312
	$(\frac{1}{16}, \frac{1}{16})$	$(\frac{\pi}{8}, \frac{\pi}{16})$	3.3051	3.2808	2.3245

Table 8. Convergence order under the three norms with $\theta = 1$ at $t = 1$.

Basis	(h_1, h_2)	(α, β)	L^∞-order	L^2-order	H^1-order
Lagrange	$(\frac{1}{2}, \frac{1}{2})$	-	-	-	-
	$(\frac{1}{4}, \frac{1}{4})$	-	2.8663	2.9813	2.1707
	$(\frac{1}{8}, \frac{1}{8})$	-	2.8908	2.9903	2.0187
	$(\frac{1}{16}, \frac{1}{16})$	-	3.0227	2.9963	2.0095
C-Bézier	$(\frac{1}{2}, \frac{1}{2})$	$(\frac{5\pi}{6}, \frac{\pi}{2})$	-	-	-
	$(\frac{1}{4}, \frac{1}{4})$	$(\frac{\pi}{2}, \frac{\pi}{4})$	3.3726	3.1919	2.1699
	$(\frac{1}{8}, \frac{1}{8})$	$(\frac{\pi}{4}, \frac{\pi}{8})$	3.3853	3.1256	2.2801
	$(\frac{1}{16}, \frac{1}{16})$	$(\frac{\pi}{8}, \frac{\pi}{16})$	3.3754	3.1134	2.0418

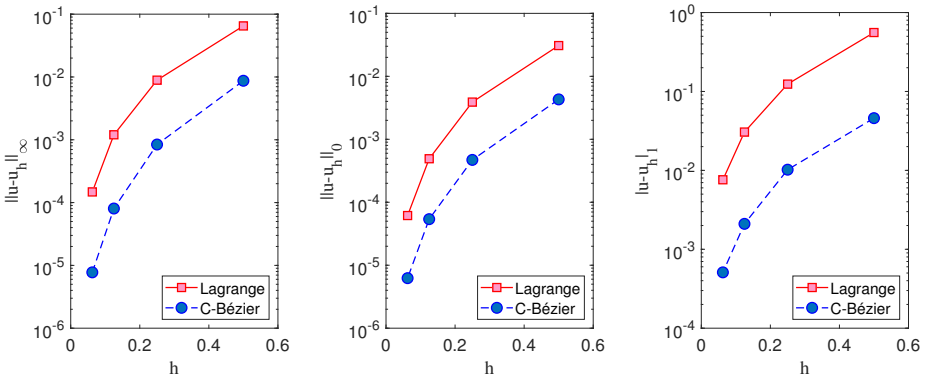

(a) $\|\boldsymbol{u}-\boldsymbol{u}_h\|_\infty$ (b) $\|\boldsymbol{u}-\boldsymbol{u}_h\|_0$ (c) $|\boldsymbol{u}-\boldsymbol{u}_h|_1$

Figure 6. The error comparison with $\theta = 0.25$ at $t = 1$.

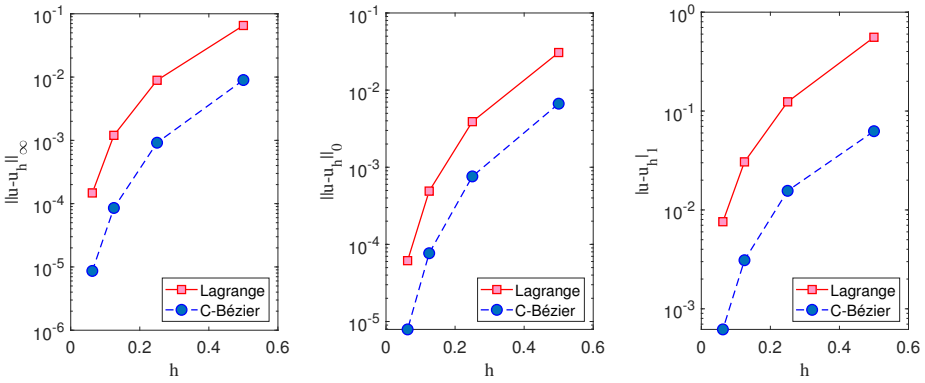

(a) $\|\boldsymbol{u}-\boldsymbol{u}_h\|_\infty$ (b) $\|\boldsymbol{u}-\boldsymbol{u}_h\|_0$ (c) $|\boldsymbol{u}-\boldsymbol{u}_h|_1$

Figure 7. The error comparison with $\theta = 1$ at $t = 1$.

The C-Bézier finite element method has higher accuracy and faster convergence rate. The accuracy of numerical results obtained by C-Bézier basis function are improved by 1–3 orders of magnitude.

6. Conclusions and future work

This article presents a detailed finite element algorithm description of how C-Bézier basis functions can be applied to give more accurate solutions for unsteady elastic equations. The error estimates and corresponding convergence order under the L^∞ norm, L^2 norm and H^1 semi-norm are obtained by numerical experiments. It is verified that the C-Bézier basis functions have higher numerical accuracy when solving unsteady elastic equations.

The accuracy of the numerical solutions is closely related to the selection of shape parameters. The determination of shape parameters is always the focus of researchers in error estimation. In the future, we will continue to study how to select the optimal shape parameters so that the numerical solutions can more effectively approximate the exact solutions.

Use of AI tools declaration

The authors declare they have not used Artificial Intelligence (AI) tools in the creation of this article.

Acknowledgements

This work was partly supported by Program for Science Technology Innovation Talents in Universities of Henan Province (No. 22HASTIT021), the Science and Technology Project of Henan Province (No. 212102210394), the National Natural Science Foundation of China (No. 11801490).

Conflict of interest

All authors declare no conflicts of interest in this paper.

References

1. S. Patnaik, S. Sidhardh, F. Semperlotti, A Ritz-based finite element method for a fractional-order boundary value problem of nonlocal elasticity, *Int. J. Solids Struct.*, **202** (2020), 398–417. https://doi.org/10.1016/j.ijsolstr.2020.05.034
2. O. A. González-Estrada, S. Natarajan, J. J. Ródenas, S. P. A. Bordas, Error estimation for the polygonal finite element method for smooth and singular linear elasticity, *Comput. Math. Appl.*, **92** (2021), 109–119. https://doi.org/10.1016/j.camwa.2021.03.017
3. A. M. Vargas, Finite difference method for solving fractional differential equations at irregular meshes, *Math. Comput. Simulat.*, **193** (2022), 204–216. https://doi.org/10.1016/j.matcom.2021.10.010
4. T. A. Bullo, G. A. Degla, G. F. Duressa, Parameter-uniform finite difference method for singularly perturbed parabolic problem with two small parameters, *Int. J. Comput. Methods Eng. Sci. Mech.*, **23** (2022), 210–218. https://doi.org/10.1080/15502287.2021.1948148
5. J. Jeon, J. Lee, S. J. Kim, Finite volume method network for the acceleration of unsteady computational fluid dynamics: Non-reacting and reacting flows, *Int. J. Energy Res.*, **46** (2022), 10770–10795. https://doi.org/10.1002/er.7879
6. U. S. Fjordholm, M. Musch, N. H. Risebro, Well-posedness and convergence of a finite volume method for conservation laws on networks, *SIAM J. Numer. Anal.*, **60** (2022), 606–630. https://doi.org/10.1137/21M145001X
7. S. Sengupta, N. A. Sreejith, P. Mohanamuraly, G. Staffelbach, L. Gicquel, Global spectral analysis of the Lax-Wendroff-central difference scheme applied to convection-diffusion equation, *Comput. Fluids*, **242** (2022), 105508. https://doi.org/10.1016/j.compfluid.2022.105508
8. R. Courant, Variational methods for the solution of problems of equilibrium and vibrations, *Bull. Amer. Math. Soc.*, **49** (1943), 1–23.
9. R. W. Clough, Y. Rashid, Finite element analysis of axi-symmetric solids, *J. Eng. Mech. Div.*, **91** (1965), 71–85. https://doi.org/10.1061/JMCEA3.0000585

10. K. Feng, Difference scheme based on variational principle, *Appl. Math. Comput.*, **2** (1965), 238–262.

11. M. I. Ivanov, I. A. Kremer, Y. M. Laevsky, Solving the pure Neumann problem by a mixed finite element method, *Numer. Anal. Appl.*, **15** (2022), 316–330. https://doi.org/10.1134/S1995423922040048

12. H. D. Gao, W. W. Sun, Optimal analysis of non-uniform Galerkin-mixed finite element approximations to the Ginzburg-Landau equations in superconductivity, *SIAM J. Numer. Anal.*, **61** (2023), 929–951. https://doi.org/10.1137/22M1483670

13. X. L. Wang, X. L. Meng, S. Y. Zhang, H. F. Zhou, A modified weak Galerkin finite element method for the linear elasticity problem in mixed form, *J. Comput. Appl. Math.*, **420** (2023), 114743. https://doi.org/10.1016/j.cam.2022.114743

14. B. Deka, N. Kumar, A systematic study on weak Galerkin finite element method for second-order parabolic problems, *Numer. Methods Partial Differ. Equ.*, **39** (2023), 2444–2474. https://doi.org/10.1002/num.22973

15. E. Chung, Y. Efendiev, Y. B. Li, Q. Li, Generalized multiscale finite element method for the steady state linear Boltzmann equation, *Multiscale Model. Simul.*, **18** (2020), 475–501. https://doi.org/10.1137/19M1256282

16. J. H. Yue, G. R. Liu, M. Li, R. P. Niu, A cell-based smoothed finite element method for multi-body contact analysis using linear complementarity formulation, *Int. J. Solids Struct.*, **141–142** (2018), 110–126. https://doi.org/10.1016/j.ijsolstr.2018.02.016

17. Y. Cheng, Q. Zhang, Local analysis of the fully discrete local discontinuous Galerkin method for the time-dependent singularly perturbed problem, *J. Comput. Math.*, **35** (2017), 265–288. https://doi.org/10.4208/jcm.1605-m2015-0398

18. J. B. Lin, H. Li, Z. M. Dong, Z. H. Zhao, Error estimations of SUPC stabilized space-time finite element approximations for convection-diffusion-reaction equations (Chinese), *Math. Appl.*, **33** (2020), 275–294. https://doi.org/ 10.13642/j.cnki.42-1184/o1.2020.02.002

19. V. D. Varma, S. K. Nadupuri, N. Chamakuri, A posteriori error estimates and an adaptive finite element solution for the system of unsteady convection-diffusion-reaction equations in fluidized beds, *Appl. Numer. Math.*, **163** (2021), 108–125. https://doi.org/10.1016/j.apnum.2021.01.012

20. Z. C. Shi, On spline finite element method, *Math. Numer. Sin.*, **1** (1979), 50–72. https://doi.org/10.12286/jssx.1979.1.50

21. T. J. R. Hughes, J. A. Cottrell, Y. Bazilevs, Isogeometric analysis: CAD, finite elements, NURBS, exact geometry and mesh refinement, *Comput. Methods Appl. Mech. Eng.*, **194** (2005), 4135–4195. https://doi.org/10.1016/j.cma.2004.10.008

22. X. Li, F. Chen, On the instability in the dimension of splines spaces over T-meshes, *Comput. Aided Geom. D.*, **28** (2011), 420–426. https://doi.org/10.1016/j.cagd.2011.08.001

23. X. Peng, H. J. Lian, Z. W. Ma, C. Zheng, Intrinsic extended isogeometric analysis with emphasis on capturing high gradients or singularities, *Eng. Anal. Bound. Elem.*, **134** (2022), 231–240. https://doi.org/10.1016/j.enganabound.2021.09.022

24. M. J. Peake, J. Trevelyan, G. Coates, Extended isogeometric boundary element method (XIBEM) for three-dimensional medium-wave acoustic scattering problems, *Comput. Methods Appl. Mech. Eng.*, **284** (2015), 762–780. https://doi.org/10.1016/j.cma.2014.10.039

25. Y. P. Zhu, X. L. Han, New cubic rational basis with tension shape parameters, *Appl. Math. J. Chin. Univ.*, **30** (2015), 273–298. https://doi.org/10.1007/s11766-015-3232-8

26. Q. Y. Chen, G. Z. Wang, A class of Bézier-like curves, *Comput. Aided Geom. D.*, **20** (2003), 29–39. https://doi.org/10.1016/S0167-8396(03)00003-7

27. C. Y. Li, C. Zhu, Designing developable C-Bézier surface with shape parameters, *Mathematics*, **8** (2020), 1–21. https://doi.org/10.3390/math8030402

28. L. Y. Sun, F. M. Su, Application of C-Bézier and H-Bézier basis functions to numerical solution of convection-diffusion equations, *Bound. Value. Probl.*, **2022** (2022), 66. https://doi.org/10.1186/s13661-022-01647-5